

RSC Advances



This is an *Accepted Manuscript*, which has been through the Royal Society of Chemistry peer review process and has been accepted for publication.

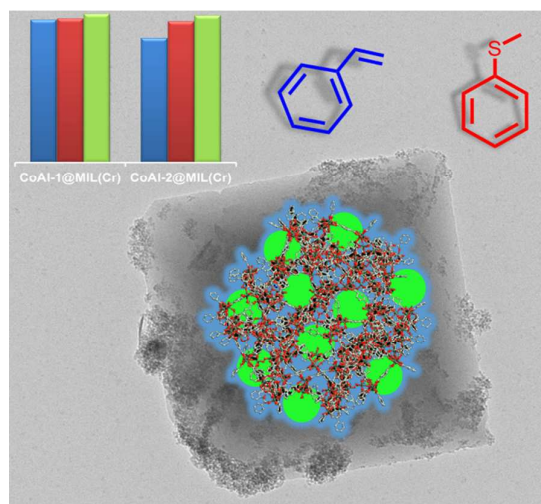
Accepted Manuscripts are published online shortly after acceptance, before technical editing, formatting and proof reading. Using this free service, authors can make their results available to the community, in citable form, before we publish the edited article. This *Accepted Manuscript* will be replaced by the edited, formatted and paginated article as soon as this is available.

You can find more information about *Accepted Manuscripts* in the [Information for Authors](#).

Please note that technical editing may introduce minor changes to the text and/or graphics, which may alter content. The journal's standard [Terms & Conditions](#) and the [Ethical guidelines](#) still apply. In no event shall the Royal Society of Chemistry be held responsible for any errors or omissions in this *Accepted Manuscript* or any consequences arising from the use of any information it contains.

Cobalt Aluminate Nanoparticles Supported on MIL-101 Structure: Catalytic Performance Investigation

Carlos M. Granadeiro,^{*} Mohamed Karmaoui, Eva Correia, Diana Julião, Vitor S. Amaral, Nuno J.O. Silva, Luís Cunha-Silva and Salette S. Balula^{*}



Novel heterogeneous catalysts composed by CoAl₂O₄ nanoparticles supported on MIL-101(Cr) framework exhibiting remarkable catalytic performance for thioanisole oxidation under sustainable conditions.

ARTICLE

Cobalt Aluminate Nanoparticles Supported on MIL-101 Structure: Catalytic Performance Investigation

Cite this: DOI: 10.1039/x0xx00000x

Carlos M. Granadeiro,^{a*} Mohamed Karmaoui,^b Eva Correia,^a Diana Julião,^a Vitor S. Amaral,^b Nuno J. O. Silva,^b Luís Cunha-Silva^a and Salette S. Balula^{a*}

Received 00th January 2012,
Accepted 00th January 2012

DOI: 10.1039/x0xx00000x

www.rsc.org/

The first catalytic active composites based in CoAl₂O₄ nanoparticles with different size (5.5 and 2.5 nm) were successfully prepared using a simple methodology of incorporation into MIL-101(Cr) framework, CoAl-x@MIL(Cr). Characterization of CoAl-x@MIL(Cr) composites by elemental analysis, vibrational spectroscopy (FT-IR and FT-Raman), powder X-ray diffraction (XRD), scanning electron microscopy (SEM), transmission electron microscopy (TEM) and energy dispersive X-ray spectroscopy (EDX) confirmed the successful preparation and stability of the support structure after nanoparticles immobilization. A remarkable catalytic performance was found for thioanisole oxidation under sustainable conditions (95% of conversion after 30 min of reaction) and the catalytic application of the most active composite was extended to styrene oxidation. Higher catalytic performance was achieved for the composite prepared with larger CoAl₂O₄ nanoparticles. The recyclability and the stability of composites after catalytic use were investigated. For the CoAl-x@MIL(Cr) catalytic systems, the loading parameter instead of the nanoparticle size seemed to have a pronounced influence in the heterogeneous catalytic performance. The confinement effect promoted by MIL-101(Cr) cavities associated to the higher number of catalytic active centers (CoAl₂O₄) is clearly more important than the size of the catalytic nanoparticles used.

Introduction

The high surface area-to-volume ratio and the intriguing properties of nanoparticles (NPs) has led to their extensive application in a wide range of fields including biomedicine, ceramics, electronics and catalysis.¹ Cobalt aluminate spinels are well known pigments used for decades in the plastics and paints industries² but more recently, cobalt aluminate nanostructured materials are being applied as catalysts,^{2,3} gas sensors⁴ and self-cleaning agents.⁵ Concerning the catalytic applications, nanostructured cobalt aluminate have shown to be active and efficient catalysts in the oxidation of alcohols,² aldol condensation^{3,6} and degradation of H₂O₂.⁵ Nevertheless, the application of transition metal aluminate nanoparticles,

especially cobalt aluminate, as active species in the design of heterogeneous catalytic systems is still relatively unexplored.

The remarkable structural and chemical diversity of porous metal-organic frameworks (MOFs) have led to their extensive application in a wide range of fields such as gas and liquid storage,⁷ magnetism,⁸ drug delivery⁹ and more recently, as solid supports for the preparation of heterogeneous catalysts.¹⁰ In particular, MOFs have been used as hosts for the immobilization of nanoparticles due to their high porosity composed by open channels and cavities allowing the nanoparticles to be accessible as well as preventing aggregation.^{11,12} These nanoparticle-embedded MOF systems have shown interesting applications in the fields of gas storage, chemical sensing and heterogeneous catalysis, namely in the oxidation of CO and alcohols, hydrogenation and C-C coupling reactions.¹¹⁻¹³

Among such diversity of MOFs, the chemical robustness and the peculiar 3-dimensional porous framework of the chromium(III) terephthalate MIL-101(Cr) with large and regular pores has led to its use as solid support in the design of novel heterogeneous catalysts.^{14,15} Several reports can be found

^aREQUIMTE& Department of Chemistry and Biochemistry, Faculty of Sciences, University of Porto, 4169-007 Porto, Portugal. E-mail: cgranadeiro@fc.up.pt, sbalula@fc.up.pt; Tel: +351 220402576; Fax: +351 220402659.

^bCICECO& Department of Physics, University of Aveiro, 3810-193 Aveiro, Portugal.

† Electronic Supplementary Information (ESI) available: additional characterization data for the CoAl-2@MIL(Cr) composite material. See DOI: 10.1039/b000000x/

in the literature describing the preparation of composite materials through the incorporation of metallic nanoparticles in the chromium(III) terephthalate MIL-101(Cr) for catalytic applications.^{11,16-19}

The increasing interest in the oxidation of organic sulfides is related with the fact that the resulting sulfoxides and sulfones are valuable intermediates in the synthesis of several pharmaceutical and agrochemical products.²⁰ Thioanisole is the most commonly used substrate when evaluating the performance of a catalyst in sulfoxidation reactions. Several reports dealing with the oxidation of thioanisole are described in the literature using metallic complexes incorporated/immobilized in different solid supports, such as silica,²¹ polymeric fibers,²² mesoporous titania,²⁰ alumina aerogels and xerogels,²³ zeolites,²⁴ as well as fullerene-based nanoconjugates²⁵ and, more recently, a three-dimensional graphene oxide foam.²⁶ Li *et al.* describe the application of thiolate-stabilized gold nanoclusters in the sulfoxidation of different organic sulfides.²⁷ The nanoclusters showed interesting catalytic activity in the sulfoxidation of thioanisole using iodobenzene as the oxidant with no significant loss of activity after five consecutive cycles.

The oxidation of styrene is of great importance for the industry since the main products obtained, i.e styrene oxide and benzaldehyde, are valuable organic intermediates for the production of fine chemicals. Environmentally friendly methods for oxidation of styrene with a clean oxidant have been a subject of current research.²⁸⁻³³ The application of metallic nanoparticles to catalyze styrene oxidation in the presence of hydrogen peroxide is not largely explored. The few work performed is based on iron oxide³² and titanium dioxide³⁴ supported in silica matrices and more recently in gold and silver nanoparticles incorporated in layered manganese oxides.³¹ The application of MOFs as heterogeneous catalysts for styrene oxidation has been investigated mainly in the presence of organic oxidants such as tert-butyl hydroperoxide, among others.³⁵⁻³⁷ Using sustainable oxidants, such as H₂O₂, scarce work can be found in the literature.^{30,38,39}

In this work we report the preparation of the first hybrid composite based on CoAl₂O₄ nanoparticles obtained through their incorporation within the porous framework of MIL-101(Cr). Different sized nanoparticles were selected, with average diameters of approximately 5.5 nm and 2.5 nm which lead to the formation of the CoAl-1@MIL(Cr) and CoAl-2@MIL(Cr) composites, respectively. The novel composites presented a remarkable catalytic activity for the sulfoxidation of thioanisole under sustainable conditions. The catalytic application of CoAl-1@MIL(Cr) was enlarged to the oxidation of styrene. The influence of the nanoparticles size in the catalytic performance was evaluated. The catalytic efficiency, robustness and recycling ability of the composites was investigated. To the best of our knowledge, this is the first work reporting the incorporation of CoAl₂O₄ nanoparticles in MOF-type materials for catalytic applications.

Results and discussion

Catalyst preparation and characterization

The composite materials were prepared through the incorporation of CoAl₂O₄ nanoparticles with average sizes of 5.5 nm and 2.5 nm in the chromium terephthalate MIL-101 framework resulting in the composites CoAl-1@MIL(Cr) and CoAl-2@MIL(Cr), respectively. These materials were extensively characterized by several characterization techniques, including elemental analysis, vibrational spectroscopy (FT-IR and FT-Raman), powder X-ray diffraction (XRD), scanning electron microscopy (SEM), transmission electron microscopy (TEM) and energy dispersive X-ray spectroscopy (EDX). The elemental analysis results indicate the presence of Co and Al from the nanoparticles with a total metal loading of 2.0 wt% and 0.54 wt% for CoAl-1@MIL(Cr) and CoAl-2@MIL(Cr), respectively. The FT-IR spectra of the composites were compared with the spectra of the MIL-101 support and the CoAl₂O₄ nanoparticles (Fig. 1A and Fig. S1, ESI†). The spectra are mainly composed by the typical absorption bands of the solid support, namely the intense bands in the 1700-1300 cm⁻¹ range assigned to $\nu_{as}(\text{COO})$, $\nu_s(\text{COO})$ and $\nu(\text{C-C})$.⁴⁰⁻⁴² Other typical bands can also be found in both spectra, such as the less intense bands ascribed to the $\delta(\text{C-H})$ and $\gamma(\text{C-H})$ stretching modes of the aromatic rings⁴⁰ located at *ca.* 1018; 748 cm⁻¹ and 991; 721 cm⁻¹ for CoAl-1@MIL(Cr) and CoAl-2@MIL(Cr), respectively. Some evidences, however, can be found regarding the presence of the nanoparticles in the final composite specially in the CoAl-1@MIL(Cr) spectrum. It is possible to observe an increase of the relative intensity of some bands, namely the bands located at 1620 and 1018 cm⁻¹, when compared with the same bands in the MIL-101 spectrum. Such fact is most likely due to the relative contribution of the nanoparticles bands that leads to the increase of the MIL-101 bands located at similar wavenumbers in the CoAl-1@MIL(Cr)spectrum. The FT-Raman spectrum of CoAl-1@MIL(Cr) (Fig. 1B) exhibits the characteristic bands arising from the MOF.⁴³ The presence of the nanoparticles in the composite is shown by a broad band (3377 cm⁻¹) assigned to the $\nu(\text{O-H})$ of water molecules together with a band located at *ca.* 3078 cm⁻¹ attributed to the $\nu(\text{C-H})$ of the phenyl rings arising from the solvent used in the nanoparticles preparation.⁴⁴ The spectrum of CoAl-2@MIL(Cr) (Fig. S2, ESI†) is nearly identical to the MIL-101(Cr), although in this case the presence of the nanoparticles is not so clear probably as a result of the lower metal loading in this composite.

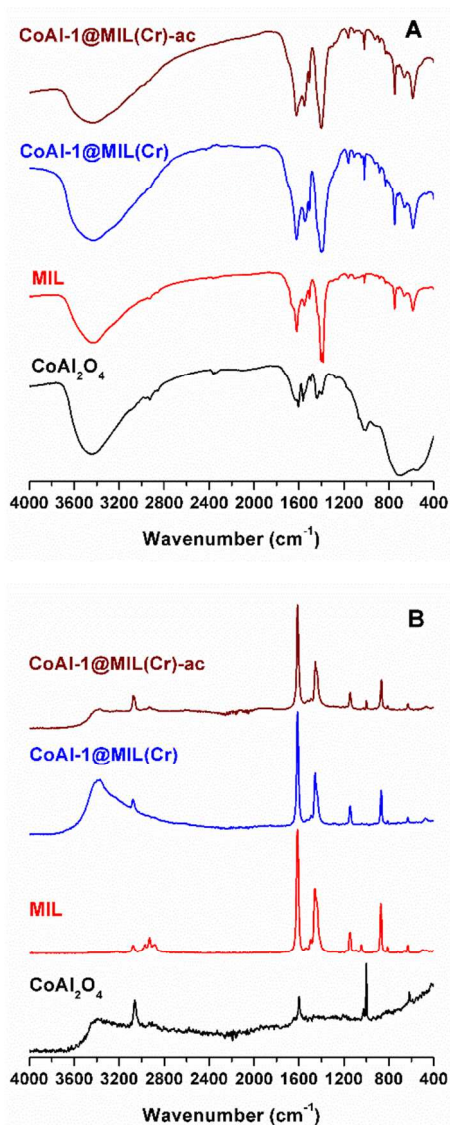


Fig. 1 FT-IR (A) and FT-Raman (B) spectra of CoAl_2O_4 nanoparticles, the solid support MIL-101 and the CoAl-1@MIL(Cr) composite before and after catalysis.

The isolated nanoparticles, the MIL-101 support and the composite materials were studied by powder XRD (Fig. 2 and Fig. S3, ESI†). In the patterns of both composites, the main diffraction peaks of the MOF [for example, $2\theta = 3.99$ (h, k, l 4, 0, 0), 5.20 (3, 3, 3), 5.84 (5, 3, 1), 8.40 (6, 6, 0), 9.00 (7, 5, 3) and 10.40 (10, 2, 2)] remain essentially unaltered after the incorporation of the nanoparticles. This fact indicates that the crystalline structure of MIL-101 is retained in the final composite materials and no collapse or degradation of the framework occurs. The absence of peaks from the nanoparticles in the CoAl-1@MIL(Cr) and CoAl-2@MIL(Cr) XRD patterns suggests a dispersion of the nanoparticles within the frameworks. In fact, the XRD patterns of the composites are dominated by the peaks of the more crystalline and abundant MOF while the broad and low intensity peaks of the nanoparticles are probably hidden in the background.

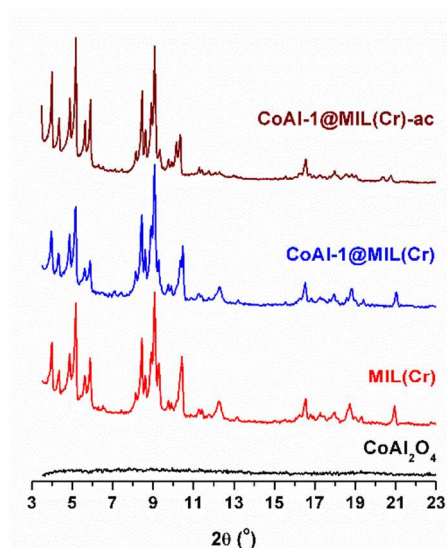


Fig. 2 Powder XRD patterns of CoAl_2O_4 nanoparticles, the solid support MIL-101 and the CoAl-1@MIL(Cr) composite before and after catalysis in the $3\text{-}23^\circ$ range.

The morphology and chemical composition of the composite materials was also assessed by electron microscopy and energy dispersive X-ray spectroscopy (EDX). For comparison purposes, the isolated nanoparticles and the solid support were also studied by electron microscopy. The SEM images (Fig. S4, ESI†) of the composite materials show the characteristic morphology of the solid support although the presence of the nanoparticles is not clear. Fig. 3a shows the HRTEM image of the CoAl_2O_4 nanoparticles with an average size of 5.5 nm exhibiting a good dispersion and a uniform quasi-spherical morphology. The HRTEM image of the solid support (Fig. 3b) shows very well-defined cubic micro-crystals which are typical of the MIL-101(Cr) morphology¹⁵ while the corresponding EDX spectrum (not shown) reveals the presence of chromium. The higher resolution obtained with the HRTEM technique allowed to observe the presence of the nanoparticles in the composite. In fact, the HRTEM images of CoAl-1@MIL(Cr) (Fig. 3c and 3d) exhibits the CoAl_2O_4 nanoparticles immobilized on the cubic micro-crystals of the solid support. Furthermore, the existence of cobalt and aluminum in the EDX spectrum (Fig. S5a, ESI†) unequivocally confirms the presence of the CoAl_2O_4 nanoparticles in the composite material.

EDX elemental mapping was also performed for the CoAl-1@MIL(Cr) composite (Fig. 4). The results indicate a uniform distribution of chromium from MIL-101 as well as the existence of the nanoparticles in the composite by showing the presence of the cobalt and aluminum elements

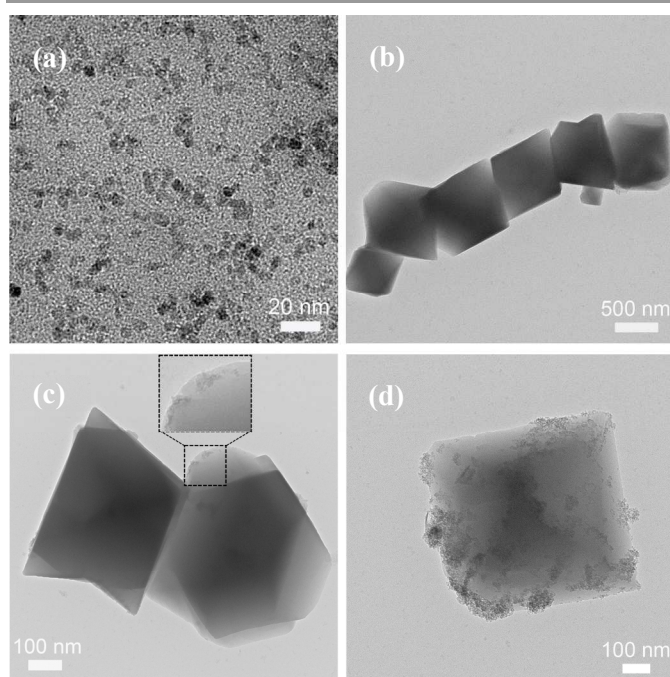


Fig. 3 HRTEM images of (a) CoAl_2O_4 nanoparticles, (b) solid support MIL-101(Cr), (c) and (d) CoAl-1@MIL(Cr) composite material.

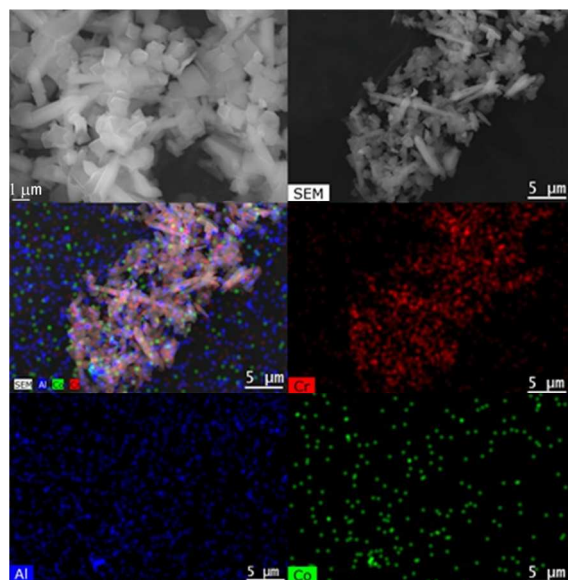
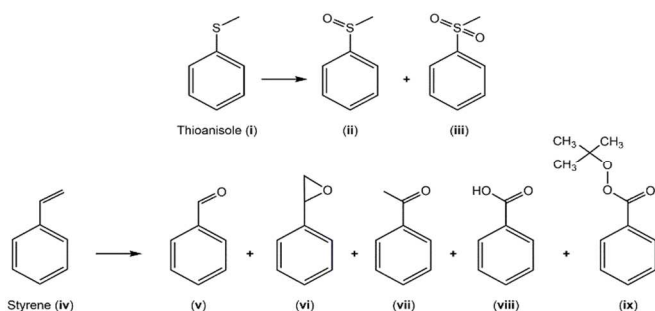


Fig.4 SEM image and elemental mapping images for CoAl-1@MIL(Cr) composite material.

Catalytic studies

The composite materials were evaluated as heterogeneous catalysts in the oxidation of thioanisole (**i**, Scheme 1). The CoAl-1@MIL(Cr) composite was also tested in the oxidation of styrene (**iv**, Scheme 1). Acetonitrile was used as the solvent and H_2O_2 or aqueous *t*-BuOOH were used as oxidants in the

oxidation of thioanisole (**i**) and styrene (**iv**), respectively. No conversion was observed using only the isolated solid support (MIL-101(Cr)) in similar catalytic conditions to the ones used in the oxidation reactions. The catalytic results obtained are summarized in Tables 1 and 2 for the oxidations of thioanisole (**i**) and styrene (**iv**), respectively. Fig. 5 compares the kinetic profiles obtained for the oxidation of thioanisole (**i**) catalyzed by CoAl-1@MIL(Cr) and CoAl-2@MIL(Cr) . These reactions were performed using the same percentage of CoAl_2O_4 active centers [6 mg of CoAl-1@MIL(Cr) and 20 mg CoAl-2@MIL(Cr)] in both composites to investigate the influence of the nanoparticle size. It is possible to observe that the composite incorporating the larger size CoAl_2O_4 nanoparticles, CoAl-1@MIL(Cr) , presented higher conversions in shorter reaction times. This is an unexpected result since it is well known that the nanoparticles with smaller dimensions usually show higher conversion.⁴⁵ However, it is also known that the activity of the nanoparticles is largely influenced by the nature of the support.⁴⁵ Since the support in both composites is the same (MIL-101(Cr)) and it is absent of catalytic activity even in the presence of high amounts (i.e 20 mg), the difference of activity observed between the composites may be related with the different loading obtained for each composite and, probably a different interaction of CoAl_2O_4 nanoparticles with the support and their stability inside the MIL-101(Cr) cavities. To further investigate this point, the oxidation of thioanisole using the isolated nanoparticles without the solid support was performed. The oxidation was carried out using equivalent amounts of nanoparticles to the ones present in the composite materials according to its metal loading. As expected, the smaller size nanoparticles (CoAl-2) exhibited a higher catalytic activity than the larger nanoparticles (CoAl-1). The comparison between the catalytic performance of the nanoparticles and the related composites (Fig. S6, ESI†) shows that the immobilization of the nanoparticles has led to an enhancement of their catalytic activity. This enhancement effect is more pronounced for the larger nanoparticles (CoAl-1) probably as a consequence of a higher nanoparticle loading. In fact, the higher nanoparticle loading of CoAl-1@MIL(Cr) composite when compared with that of CoAl-2@MIL(Cr) may be responsible for the different conversion values observed. In CoAl-1@MIL(Cr) , the higher number of catalytic active centers present per cavity of MIL-101(Cr) could result in a more pronounced confinement effect.^{39,46} In this case, more frequent interactions between the active centers and the substrates will occur which could lead to higher conversion values.



Scheme 1. Schematic representation of the oxidation products for the different substrates.

Table 1. Catalytic data for the oxidation of thioanisole^a using the heterogeneous catalysts.

	Time (h)	Conversion (%)	Selectivity ^b (%)		
			ii	iii	
CoAl-1@MIL(Cr)	1 st cycle	0.17	46	70	30
		0.5	95	68	32
	2 nd cycle	0.17	45	42	58
		0.5	96	71	29
	3 rd cycle	0.17	44	80	20
		0.5	99	76	24
CoAl-2@MIL(Cr)	1 st cycle	0.17	42	48	52
		0.5	83	95	5
	2 nd cycle	0.17	86	100	-
		0.5	94	100	-
	3 rd cycle	0.17	97	100	-
		0.5	98	100	-

^aReaction conditions: 0.5 mmol of substrate, 2 mmol H₂O₂, 6 mg of CoAl-1@MIL(Cr) or 20 mg of CoAl-2@MIL(Cr), 1.0 mL CH₃CN at 70 °C. ^bBased on the amount of consumed substrate.

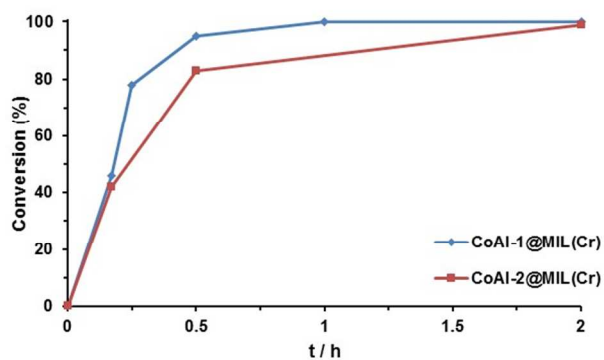


Fig. 5 Kinetic profile for the oxidation of thioanisole using CoAl-1@MIL(Cr) and CoAl-2@MIL(Cr) heterogeneous catalysts.

For the oxidation of thioanisole (i), a practically complete conversion (95%) was attained using CoAl-1@MIL(Cr) after only 30 min of reaction with 65% of selectivity towards methylphenylsulfoxide (ii). For the same reaction time, using CoAl-2@MIL(Cr) has led to a 83% conversion and 95% selectivity towards methylphenylsulfoxide (ii). Some examples

can be found in the literature dealing with the oxidation of thioanisole catalyzed by metallic nanoparticles.^{27,47,48} Despite reporting practically complete conversions in the oxidation of thioanisole, the catalysts require much longer reactions times than the CoAl-x@MIL(Cr) composites herein reported. Although having a higher surface area, the smaller nanoparticles (ca. 2.5 nm) in CoAl-2@MIL(Cr) have shown similar or even inferior catalytic activity than the nanoparticles (ca. 5.5 nm) in CoAl-1@MIL(Cr). The extremely fast reaction rate of this oxidation together with the confinement effect promoted by the cages of MIL-101(Cr) are probably responsible for the similar activity observed of both composites despite the different size of the nanoparticles.

The slightly better catalytic performance of the CoAl-1@MIL(Cr) composite has motivated its application in a different catalytic reaction, namely in the oxidation of styrene (iv). The use of CoAl-1@MIL(Cr) resulted in an 89% conversion after 30h of reaction with 48% selectivity towards benzaldehyde (v). As shown in Table 2, after 2h of reaction only benzaldehyde (v, 50%) and styrene oxide (vi, 50%) are formed. However, at the end of the reaction (30h) other oxidation products are observed: acetophenone (vii, 6%), benzoic acid (viii, 3%) and *t*-butylperoxybenzoate (ix, 10%). Until the first 2h of reaction, the only products obtained are benzaldehyde (v) and styrene oxide (vi) in approximately equal amounts. For this reason, the other oxidation products (acetophenone, benzoic acid and *t*-butylperoxybenzoate), that are only present after the initial 6h of reaction, should be formed through the further oxidation of the first two oxidation products (benzaldehyde and styrene oxide). The gradual decrease in the selectivity values of benzaldehyde and styrene oxide after the initial 6h of reaction, should indicate that the later oxidation products are probably formed through the subsequent oxidation of the two initial products. This reaction path is consistent with reports in the literature dealing with the oxidation of styrene using *t*-BuOOH as the oxidant. Choudhary *et al.* describe the oxidation of styrene using supported gold nanoparticles as heterogeneous catalysts.⁴⁹ In fact, the authors were able to conclude that benzaldehyde and styrene oxide are the primary products in the oxidation of styrene while the remaining products are formed through the oxidation of these primary products. Other publications reporting the catalytic oxidation of styrene with *t*-BuOOH as the oxidant also attribute the decrease in the selectivity of styrene oxide that usually occurs after long reactional times (>12h) to its decomposition into benzaldehyde, acetophenone and benzoic acid.^{50,51}

As previously performed, the catalytic activity of the isolated nanoparticles was also evaluated in the oxidation of styrene using identical experimental conditions. The results obtained reveal that the immobilization of the nanoparticles besides the advantage of allowing the recycling of the catalyst also enhances its catalytic performance towards the oxidation of styrene (Fig. S7, ESI†).

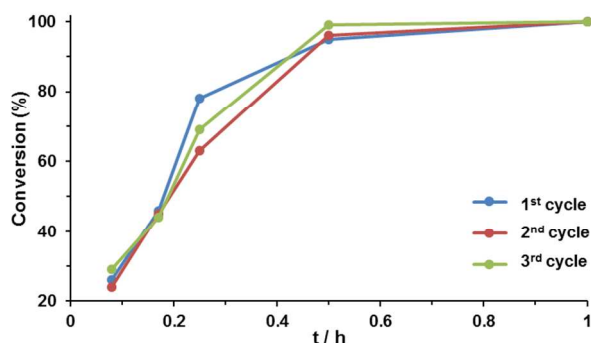
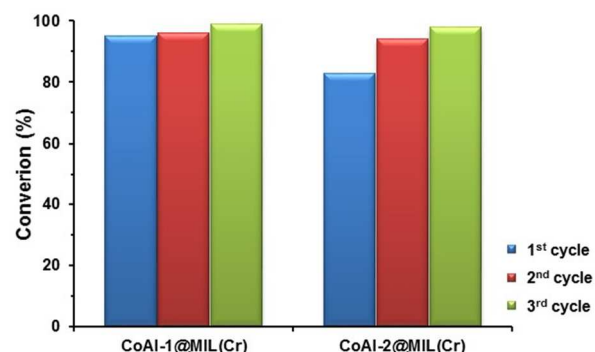
Table 2. Catalytic data for the oxidation of styrene^a using the CoAl-1@MIL(Cr) heterogeneous catalyst.

	Time (h)	Conversion (%)	Selectivity ^b (%)				
			v	vi	vii	viii	ix
CoAl-1@MIL(Cr) 1st cycle	2	8	50	50	-	-	-
	6	26	42	54	-	-	4
	30	89	48	33	6	3	10
2nd cycle	2	8	50	50	-	-	-
	6	21	43	57	-	-	-
	30	87	39	34	8	5	14
3rd cycle	2	8	88	13	-	-	-
	6	22	73	27	-	-	-
	30	93	33	-	11	1	55

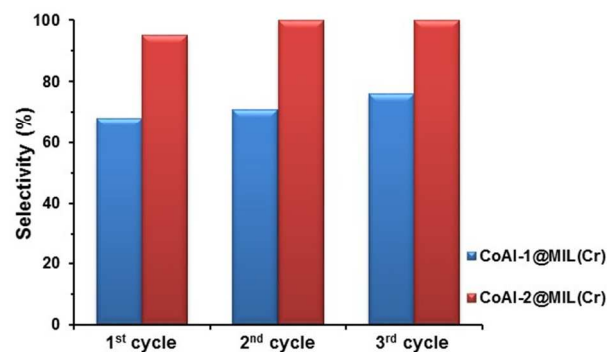
^aReaction conditions: 1 mmol of substrate, 4.5mmol *t*-BuOOH, 20 mg of catalyst, 1.5 mL CH₃CN at 70 °C. ^bBased on the amount of consumed substrate.

Recyclability and leaching

The recyclability of the composite materials was evaluated for the oxidative reactions previously described. After each catalytic cycle, the catalysts were recovered by centrifugation, washed thoroughly with acetonitrile and dried in a desiccator over silica gel. The solids were then reused in a new oxidation reaction using the same experimental conditions. The catalytic data for the second and third cycles is summarized in Table 1 and Table 2 for the oxidation of thioanisole (i) and styrene (iv), respectively. Fig. 6 shows the conversion values obtained for three consecutive cycles in the oxidation of thioanisole (i) using CoAl-1@MIL(Cr). The kinetic profiles for the three cycles are practically similar. As shown in Table 1, the selectivity values throughout the catalytic cycles also remain essentially unaltered. In fact, besides the similar conversion values, the selectivity values for the two products formed, methylphenylsulfoxide (ii) and methylphenylsulfone (iii), are identical. The conversion values obtained with both composites in the oxidation of thioanisole (i) are very similar along the catalytic cycles (Fig. 7).

**Fig. 6** Kinetic profile for three consecutive catalytic cycles for the oxidation of thioanisole using CoAl-1@MIL(Cr) as the catalyst.**Fig. 7** Conversion data obtained for three consecutive cycles in the oxidation of thioanisole after 30 min of reaction using both catalysts.

The CoAl-2@MIL(Cr) composite has shown a higher selectivity towards methylphenylsulfoxide (ii) throughout the three catalytic cycles than CoAl-1@MIL(Cr) (Fig. 8). The high reproducibility observed in all oxidative reactions clearly confirms the robustness and reusability of the heterogeneous catalysts in the oxidation of this substrate.

**Fig. 8** Selectivity towards methylphenylsulfoxide (ii) obtained for the oxidation of thioanisole using both catalysts after 30 min of reaction.

The reusability of CoAl-1@MIL(Cr) was also investigated for the oxidation of styrene (iv) in order to evaluate its versatility as heterogeneous catalyst. Fig. 9 exhibits the kinetic profiles for the oxidation of styrene with CoAl-1@MIL(Cr) and *t*-BuOOH for three consecutive cycles. The high recycling ability of the composite can be observed from the very similar kinetic profiles throughout the catalytic cycles. This similarity is consistent with a high robustness of the heterogeneous catalyst since it strongly indicates that no chemical decomposition/degradation occurs during the cycles. As shown in Table 2, conversion values of 87 % or higher were achieved after 30 h of reaction in the three cycles. Fig. 10 compares the conversion and selectivity towards benzaldehyde (v) values obtained in the oxidation of styrene with *t*-BuOOH for three consecutive cycles. The conversion values along the catalytic cycles are similar, but there is a slight decrease in the selectivity along the catalytic cycles. In fact, while the major product obtained in the oxidation of styrene in the first two cycles is

benzaldehyde (v), in the third cycle the main oxidation product is *t*-butylperoxybenzoate (ix). As previously discussed, this behavior is due to the decomposition of benzaldehyde and styrene oxide that occurs after long reactional times.

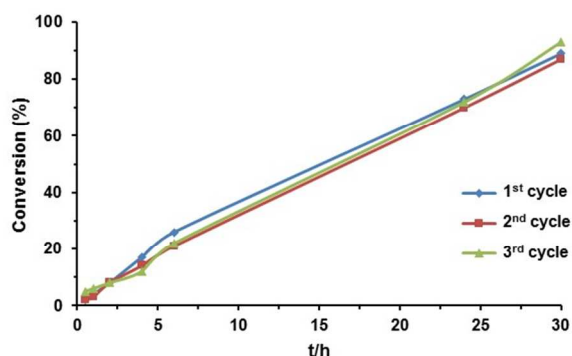


Fig. 9 Kinetic profile for three consecutive catalytic cycles for the oxidation of styrene using CoAl-1@MIL(Cr).

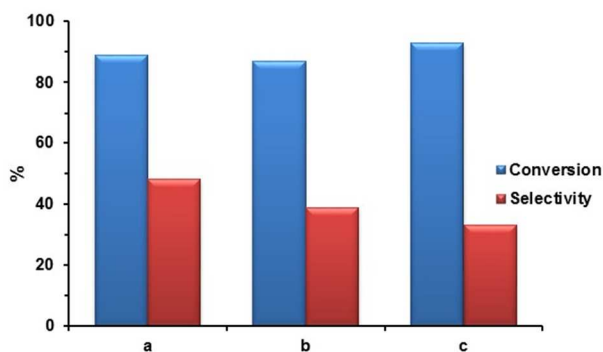


Fig. 10 Conversion and selectivity towards benzaldehyde (v) data obtained for the oxidation of styrene using CoAl-1@MIL(Cr) after 30h for the (a) first, (b) second and (c) third cycles.

The CoAl-1@MIL(Cr) composite has shown to be an active and recyclable heterogeneous catalyst in both thioanisole and styrene oxidation reactions for three consecutive cycles. In particular, the composite exhibited a remarkable catalytic activity towards the thioanisole oxidation using H_2O_2 as the oxidant (conversions higher than 95% for 30 min of reaction) when compared with the majority of reports found in the literature. Walmsley *et al.* have reported the application of oxovanadium(IV)-functionalized polybenzimidazolenanofibres as heterogeneous catalyst in the oxidation of thioanisole exhibiting interesting catalytic activity and recyclability.²² Similar conversion and selectivity values to our work were attained along three catalytic cycles, although for three times longer reaction times.

Catalyst material stability

The stability of the heterogeneous catalysts was investigated through the extensive characterization of the solid recovered after three consecutive cycles of thioanisole oxidation, CoAl-1@MIL(Cr)-ac (ac stands for after catalysis). The vibrational

spectroscopy (Fig. 1) spectra of CoAl-1@MIL(Cr)-ac are very similar to the corresponding ones before catalysis. One exception is the appearance of the nanoparticles most intense band (1001 cm^{-1}) in the Raman spectrum of the composite after catalysis (Fig. 1B). This band is absent in the corresponding spectrum before catalysis as a result of the incorporation of the nanoparticles within the MIL-101 framework. Therefore, the appearance of this band in the spectrum after catalysis should be related with the occurrence of some leaching of the nanoparticles during the catalytic cycles. In fact, the elemental analysis results indicate a Al/Cr(wt%) ratio of 0.05 for CoAl-1@MIL(Cr)-ac which is slightly lower than the ratio obtained before catalysis (0.075). The XRD pattern of the composite after catalysis (Fig. 2) exhibits a very similar profile to the pattern of CoAl-1@MIL(Cr) regarding the position and intensity of the main peaks of MIL-101(Cr) suggesting that the MOF structure is preserved after the three catalytic cycles. The morphology of the composite seems to be preserved after the catalytic cycles as the SEM images of CoAl-1@MIL(Cr)-ac (Fig. S8, ESI†) still exhibit the characteristic cubic micro-crystals of MIL-101. The EDX spectrum of CoAl-1@MIL(Cr)-ac (Fig. S5b, ESI†) also shows the presence of the elements that compose the nanoparticles (Co and Al) in a similar ratio to the EDX spectrum before catalysis. The stability of the CoAl_2O_4 nanoparticles was also evaluated by determining its size distribution (through HRTEM images analysis) in the CoAl-1@MIL(Cr) composite after three catalytic cycles of styrene oxidation. The average size of the nanoparticles before catalytic use was $4.7 \pm 0.8\text{ nm}$ while the corresponding value after the catalytic cycles was $4.2 \pm 0.6\text{ nm}$. Such a result indicates that no significant nanoparticle aggregation occurs which is consistent with the highly reproducible kinetic profiles obtained in the three styrene oxidation cycles.

Conclusions

Novel hybrid composite materials, CoAl-*x*@MIL(Cr), were prepared through the incorporation of CoAl_2O_4 nanoparticles ($x = 1$ for 5.5 nm; $x = 2$ for 2.5 nm average sizes) within the MIL-101(Cr) framework. The successful incorporation of the nanoparticles and the structural preservation of the metal-organic framework was confirmed by a vast number of characterization techniques, including vibrational spectroscopy (FT-IR and FT-Raman), elemental analysis, powder XRD, transmission and scanning electron microscopy (TEM/SEM) and energy dispersive X-ray spectroscopy (EDS) elemental mapping. The composites were tested as heterogeneous catalysts in oxidative reactions, namely in the oxidations of thioanisole and styrene.

The composite materials have proved to be efficient catalysts for oxidative catalysis, specially in the oxidation of thioanisole with practically complete conversions achieved after only 30 min of reaction. The similar catalytic data (conversion and selectivity) obtained in three consecutive catalytic cycles clearly suggests a high recycling ability of the composite. In this work, the size of the nanoparticles seems not to

significantly influence the catalytic performance of the composites. The integrity of CoAl-1@MIL(Cr) was confirmed after three consecutive catalytic cycles by different characterization techniques. Following the interesting catalytic activity and robustness exhibited by CoAl₂O₄-containing composites, we are currently interested in the design of novel composites through the encapsulation/intercalation of these nanoparticles in other solid supports and their evaluation as heterogeneous catalysts.

Experimental

Materials and methods

All the reagents used in the preparation of the composite material, such as chromium(III) nitrate nonahydrate [Cr(NO₃)₃·9H₂O, Aldrich], benzene-1,4-dicarboxylic acid (C₈H₆O₂, Aldrich), hydrofluoric acid (HF, Aldrich), cobalt acetate [(CH₃CO₂)₂Co, Aldrich], benzyl alcohol (C₇H₈O, Aldrich) and aluminiumisopropoxide [Al(OC₃H₇)₃, Aldrich] were used as received without further purification. The reagents used in the catalytic studies, namely thioanisole (Aldrich), styrene (Aldrich), acetonitrile (Panreac), hydrogen peroxide 30% (H₂O₂, Riedel-de-Häen) and aqueous *tert*-butylhydroperoxide (*t*-BuOOH, Aldrich) were used as received without further purification.

Elemental analyses for Co, Al and Cr were performed by ICP-MS at the Central Laboratory of Analyses of the University of Aveiro. FT-IR spectra were obtained on a Jasco 460 Plus spectrometer using KBr pellets, while the FT-Raman spectra were acquired on a RFS-100 Bruker FT-spectrometer, equipped with Nd:YAG laser with a 1064 nm excitation wavelength and laser power set to 350 mW. Powder X-ray diffraction patterns were obtained at room temperature on a X'Pert MPD Philips diffractometer, equipped with an X'Celerator detector and a flat-plate sample holder in a Bragg-Brentano para-focusing optics configuration (45kV, 40 mA). Intensity data were collected by the step-counting method (step 0.013°), in continuous mode, in the ca. 10 ≤ 2θ ≤ 70° range. Scanning electron microscopy (SEM) images were acquired in a high resolution scanning electron microscope Hitachi SU-70 instrument working at 4 kV.

High resolution transmission electron microscopy (HRTEM) was performed using a JEOL 2200FS microscope with a field emission gun operating at 300 kV. The energy-dispersive X-ray spectroscopy (EDX) data were collected on a Hitachi S-4100 field emission gun tungsten filament instrument working at 25 kV. Samples were analyzed as powders and prepared by deposition on aluminium sample holders followed by carbon coating using a Emitech K950 carbon evaporator. The average diameter of the nanoparticles was determined by analysis of HRTEM images using the software ImageJ v1.48 (at least 50 measurements for each case). GC-MS analysis were performed using a Hewlett Packard 5890 chromatograph equipped with a Mass Selective Detector MSD series II using helium as the carrier gas (35 cm⁻¹); GC-FID was carried out in

a Varian CP-3380 chromatograph to monitor the catalytic reactions. The hydrogen was used as the carrier gas (55 cm⁻¹) and fused silica Supelco capillary columns SPB-5 (30m × 0.25mm i.d.; 25 μm film thickness) were used.

Synthesis and preparation of the materials

CoAl₂O₄ nanoparticles. The nanoparticles were prepared through a non-aqueous sol-gel method following a recently published procedure.³² The synthesis was carried out in a glovebox (O₂ and H₂O < 1 ppm). Briefly, in a glovebox, aluminium isopropoxide (2 mmol) was added to a cobalt acetate solution (1 mmol) in benzyl alcohol (20 mL) and allowed to stir for 10 min at room temperature. The mixture is then transferred to a stainless steel autoclave and placed in an oven for 2 days at 150°C or 250 °C for the 2.5 nm and 5.5 nm nanoparticles, respectively. The suspension was centrifuged and the resulting solid was thoroughly washed with ethanol and dichloromethane, and dried in an oven at 60 °C.

Solid support MIL-101(Cr). The porous metal-organic framework (MOF) material was prepared by an adaptation of the method described by Férey *et al.*¹⁴ Briefly, a mixture containing chromium(III) nitrate (2 mmol), benzene-1,4-dicarboxylic acid (2 mmol) and hydrofluoric acid (100 μL) in H₂O (10 mL) was stirred at room temperature for homogenization, transferred to an autoclave and heated at 220°C for 9 h in an electric oven. After cooling to room temperature, the solid was recovered by centrifugation and purified through a double DMF and ethanol treatments.

Composite materials CoAl-x@MIL(Cr). The composite materials were prepared through the immobilization of the CoAl₂O₄ nanoparticles in the porous MIL-101(Cr). The nanoparticles (10 mg) were dispersed in ethanol (50 mL) and added to MIL-101(Cr) (240 mg). The mixture was stirred at room temperature for 24 h. Afterwards, the solid was isolated by centrifugation, washed thoroughly with ethanol and dried in a desiccator over silica gel. The incorporation with 5.5 nm and 2.5 nm nanoparticles lead to the formation of the CoAl-1@MIL(Cr) and CoAl-2@MIL(Cr) composites, respectively.

CoAl-1@MIL(Cr): Anal. Found (%): Cr, 10.6; Co, 1.2; Al, 0.80; total metal loading: 2.0 wt%. Selected FT-IR (cm⁻¹): 3431, 1620, 1547, 1506, 1400, 1378, 1161, 1109, 1043, 1018, 885, 829, 748, 715, 660, 586. Selected FT-Raman (cm⁻¹): 3377, 3078, 1613, 1456, 1146, 868, 812, 631.

CoAl-2@MIL(Cr): Anal. Found (%): Cr, 14.4; Co, 0.34; Al, 0.20; total metal loading: 0.54 wt%. Selected FT-IR (cm⁻¹): 3408, 1597, 1514, 1481, 1379, 1358, 1142, 1084, 1014, 991, 856, 806, 721, 688, 642, 565. Selected FT-Raman (cm⁻¹): 3080, 2934, 1615, 1460, 1148, 1044, 870, 812, 631.

Catalytic studies

The oxidation reactions (Scheme 1) were carried out in borosilicate 10 mL reaction vessels using acetonitrile (MeCN)

as the solvent. In the oxidation of thioanisole (i), the substrate (0.5 mmol) and the catalyst [6 mg for CoAl-1@MIL(Cr) or 20 mg for CoAl-2@MIL(Cr)] were dissolved in MeCN (1.0 mL) under stirring and then H₂O₂ 30% (2mmol) was added to the reaction mixture. Regarding the oxidative reaction of styrene (iv), the substrate (1 mmol) and the catalyst (20 mg) were added to MeCN (1.5 mL) under stirring followed by the addition of aqueous *t*-BuOOH (4.5 mmol). All oxidative reactions were carried out at 70°C. GC analysis was used to monitor the catalytic reactions and stopped when product yields remained constant after two successive GC analyses. An aliquot was taken directly from the reaction mixture with a microsyringe at regular intervals, diluted in acetonitrile and injected into the GC or GC-MS equipment for analysis of the starting material and products. The reaction products were identified by GC-MS analysis.

Acknowledgements

This work was partly financed by FEDER (Fundo Europeu de Desenvolvimento Regional) through COMPETE (Programa Operacional Factores de Competitividade) and by national funds through the FCT (Fundação para a Ciência e a Tecnologia) within the projects FCOMP-01-0124-FEDER-020658 (FCT ref. PTDC/EQU-EQU/121677/2010), FCOMP-01-0124-FEDER-013026 (FCT ref. PTDC/CTM/100357/2008), CICECO - FCOMP-01-0124-FEDER-037271 (FCT ref. PEst-C/CTM/LA0011/2013) and Requite - FCOMP-01-0124-FEDER-037285 (FCT ref. PEst-C/EB/LA0006/2013), and the fellowships SFRH/BPD/73191/2010 (to CG) and SFRH/BPD/74477/2010 (to MK).

References

1. R. Ghosh Chaudhuri and S. Paria, *Chem. Rev.*, 2012, **112**, 2373-2433.
2. R. T. Kumar, N. C. Sagaya Selvam, T. Adinaveen, L. J. Kennedy and J. J. Vijaya, *Reac Kinet Mech Cat*, 2012, **106**, 379-394.
3. W. Xu, X. Liu, J. Ren, P. Zhang, Y. Wang, Y. Guo, Y. Guo and G. Lu, *Catal. Commun.*, 2010, **11**, 721-726.
4. C. R. Michel, *Sens. Actuators, B*, 2010, **147**, 635-641.
5. A. Dandapat and G. De, *ACS Appl. Mater. Interfaces*, 2012, **4**, 228-234.
6. W. Xu, X. Liu, J. Ren, H. Liu, Y. Ma, Y. Wang and G. Lu, *Microporous Mesoporous Mater.*, 2011, **142**, 251-257.
7. X. Wang, L. Liu and A. J. Jacobson, *Angew. Chem. Int. Ed.*, 2006, **45**, 6499-6503.
8. D. Maspoch, D. Ruiz-Molina, K. Wurst, N. Domingo, M. Cavallini, F. Biscarini, J. Tejada, C. Rovira and J. Veciana, *Nature Mater.*, 2003, **2**, 190-195.
9. P. Horcajada, C. Serre, M. Vallet-Regí, M. Sebban, F. Taulelle and G. Férey, *Angew. Chem. Int. Ed.*, 2006, **45**, 5974-5978.
10. A. Corma, H. Garcia and F. X. Llabrés i Xamena, *Chem. Rev.*, 2010, **110**, 4606-4655.
11. M. Meilikhov, K. Yusenko, D. Esken, S. Turner, G. Van Tendeloo and R. A. Fischer, *Eur. J. Inorg. Chem.*, 2010, **2010**, 3701-3714.
12. H. R. Moon, D.-W. Lim and M. P. Suh, *Chem. Soc. Rev.*, 2013, **42**, 1807-1824.
13. H.-L. Jiang and Q. Xu, *Chem. Commun.*, 2011, **47**, 3351-3370.
14. G. Férey, C. Mellot-Draznieks, C. Serre, F. Millange, J. Dutour, S. Surblé and I. Margiolaki, *Science*, 2005, **309**, 2040-2042.
15. C. M. Granadeiro, A. D. S. Barbosa, P. Silva, F. A. A. Paz, V. K. Saini, J. Pires, B. de Castro, S. S. Balula and L. Cunha-Silva, *Appl. Catal., A*, 2013, **453**, 316-326.
16. B. Yuan, Y. Pan, Y. Li, B. Yin and H. Jiang, *Angew. Chem. Int. Ed.*, 2010, **49**, 4054-4058.
17. Y. Huang, Z. Lin and R. Cao, *Chem. Eur. J.*, 2011, **17**, 12706-12712.
18. J. Hermannsdörfer and R. Kempe, *Chem. Eur. J.*, 2011, **17**, 8071-8077.
19. Y. Pan, B. Yuan, Y. Li and D. He, *Chem. Commun.*, 2010, **46**, 2280-2282.
20. S. S. Negi, K. Sivarajani, A. P. Singh and C. S. Gopinath, *Appl. Catal., A*, 2013, **452**, 132-138.
21. M. Ghorbanloo, M. Jaworska, P. Paluch, G.-D. Li and L.-J. Zhou, *Transition Met. Chem.*, 2013, **38**, 511-521.
22. R. S. Walmsley, P. Hlangothi, C. Litwinski, T. Nyokong, N. Torto and Z. R. Tshentu, *J. Appl. Polym. Sci.*, 2013, **127**, 4719-4725.
23. N. Moussa, J. M. Fraile, A. Ghorbel and J. A. Mayoral, *J. Mol. Catal. A: Chem.*, 2006, **255**, 62-68.
24. M. R. Maurya, B. Singh, P. Adão, F. Avecilla and J. Costa Pessoa, *Eur. J. Inorg. Chem.*, 2007, **2007**, 5720-5734.
25. A. W. Jensen, B. S. Maru, X. Zhang, D. K. Mohanty, B. D. Fahlman, D. R. Swanson and D. A. Tomalia, *Nano Lett.*, 2005, **5**, 1171-1173.
26. G. A. B. Goncalves, S. M. G. Pires, M. M. Q. Simoes, G. Neves and P. Marques, *Chem. Commun.*, 2014, **50**, 7673-7676.
27. G. Li, H. Qian and R. Jin, *Nanoscale*, 2012, **4**, 6714-6717.
28. C. Chiappe, A. Sanzone and P. J. Dyson, *Green Chem.*, 2011, **13**, 1437-1441.
29. S. Ribeiro, L. Cunha-Silva, S. S. Balula and S. Gago, *New J. Chem.*, 2014, **38**, 2500-2507.
30. C. M. Granadeiro, P. Silva, V. K. Saini, F. A. A. Paz, J. Pires, L. Cunha-Silva and S. S. Balula, *Catal. Today*, 2013, **218-219**, 35-42.
31. M. M. Najafpour, M. Amini, D. J. Sedigh, F. Rahimi and M. Bagherzadeh, *RSC Advances*, 2013, **3**, 24069-24074.
32. F. Rajabi, N. Karimi, M. R. Saidi, A. Primo, R. S. Varma and R. Luque, *Adv. Synth. Catal.*, 2012, **354**, 1707-1711.
33. S. Parihar, S. Pathan, R. N. Jadeja, A. Patel and V. K. Gupta, *Inorg. Chem.*, 2012, **51**, 1152-1161.
34. D. S. Gopala, R. R. Bhattacharjee, R. Haerr, B. Yeginoglu, O. D. Pavel, B. Cojocar, V. I. Parvulescu and R. M. Richards, *ChemCatChem*, 2011, **3**, 408-416.
35. H.-F. Yao, Y. Yang, H. Liu, F.-G. Xi and E.-Q. Gao, *J. Mol. Catal. A: Chem.*, 2014, **394**, 57-65.
36. D. H. Lee, S. Kim, M. Y. Hyun, J.-Y. Hong, S. Huh, C. Kim and S. J. Lee, *Chem. Commun.*, 2012, **48**, 5512-5514.
37. M.-H. Xie, X.-L. Yang and C.-D. Wu, *Chem. Commun.*, 2011, **47**, 5521-5523.
38. S. S. Balula, C. M. Granadeiro, A. D. S. Barbosa, I. C. M. S. Santos and L. Cunha-Silva, *Catal. Today*, 2013, **210**, 142-148.
39. N. V. Maksimchuk, K. A. Kovalenko, S. S. Arzumanov, Y. A. Chesalov, M. S. Melgunov, A. G. Stepanov, V. P. Fedin and O. A. Kholdeeva, *Inorg. Chem.*, 2010, **49**, 2920-2930.

ARTICLE

40. N. V. Maksimchuk, M. N. Timofeeva, M. S. Melgunov, A. N. Shmakov, Y. A. Chesalov, D. N. Dybtsev, V. P. Fedin and O. A. Kholdeeva, *J. Catal.*, 2008, **257**, 315-323.
41. S. H. Jung, J. H. Lee, J. W. Yoon, C. Serre, G. Férey and J. S. Chang, *Adv. Mater.*, 2007, **19**, 121-124.
42. S. Ribeiro, C. M. Granadeiro, P. Silva, F. A. Almeida Paz, F. F. de Biani, L. Cunha-Silva and S. S. Balula, *Catal. Sci. Technol.*, 2013, **3**, 2404-2414.
43. O. V. Zalomaeva, K. A. Kovalenko, Y. A. Chesalov, M. S. Mel'gunov, V. I. Zaikovskii, V. V. Kaichev, A. B. Sorokin, O. A. Kholdeeva and V. P. Fedin, *Dalton Trans.*, 2011, **40**, 1441-1444.
44. M. Karmaoui, N. J. O. Silva, V. S. Amaral, A. Ibarra, A. Millan and F. Palacio, *Nanoscale*, 2013, **5**, 4277-4283.
45. Z. L. Li, J. H. Liu, C. G. Xia and F. W. Li, *ACS Catal.*, 2013, **3**, 2440-2448.
46. L. Bromberg, Y. Diao, H. Wu, S. A. Speakman and T. A. Hatton, *Chem. Mater.*, 2012, **24**, 1664-1675.
47. S. K. Karmee, L. Greiner, A. Kraynov, T. E. Muller, B. Niemeijer and W. Leitner, *Chem. Commun.*, 2010, **46**, 6705-6707.
48. W. Wang, Y. Xu, D. I. C. Wang and Z. Li, *J. Am. Chem. Soc.*, 2009, **131**, 12892-12893.
49. V. R. Choudhary, D. K. Dumbre, N. S. Patil, B. S. Uphade and S. K. Bhargava, *J. Catal.*, 2013, **300**, 217-224.
50. Y. Liu, H. Tsunoyama, T. Akita and T. Tsukuda, *Chem. Commun.*, 2010, **46**, 550-552.
51. N. Linares, C. P. Canlas, J. Garcia-Martinez and T. J. Pinnavaia, *Catal. Commun.*, 2014, **44**, 50-53.